J|A|C|S
ARTICLES
Published on Web 05/17/2002

Arresting Butterfly-Like Intermediate Nanocrystals of β-Co(OH)$_2$ via Ethylenediamine-Mediated Synthesis

Jeyagowry T. Sampanthar and Hua Chun Zeng*

Contribution from the Department of Chemical and Environmental Engineering, Faculty of Engineering, and Chemical and Process Engineering Center, National University of Singapore, 10 Kent Ridge Crescent, Singapore 119260

Received November 26, 2001

Abstract: A synthesis of β-Co(OH)$_2$ nanocrystalline materials has been investigated with the assistance of chelating agent ethylenediamine. By controlling precipitation processes, various forms of β-Co(OH)$_2$ crystallites can be prepared at different stages. The crystallite morphologies include two-dimensional hexagonal sheet platelets, one-dimensional nanorods, and butterfly-like nanocrystallite intermediates. In particular, a triangular construction unit for β-Co(OH)$_2$ crystallites has been revealed with the ethylenediamine mediation in the synthesis. With the successful arrest of these butterfly-like intermediate crystallites, especially of linearly aligned "butterflies", the formation mechanism of one-dimensional nanorods or nanoribbons has been experimentally explained. The chemical composition of solution precursors and resultant β-Co(OH)$_2$ crystallites has been analyzed with UV−vis/FTIR/CHN /XRD/TGA/TEM/SAED methods. The relationships among various observed crystallite morphologies have also been discussed on the basis of the experimental findings.

Introduction

Over the past decade, research in synthesis of low-dimensional nanostructures has become a focal area in development of novel optical, electronic, magnetic, and catalytic materials.[1−26] In particular, one-dimensional nanotubular and rodlike (whiskers) morphologies of various elemental and compound materials have been synthesized with different methods.[1−26] Interestingly, these elemental/compound materials often have hexagonal crystal symmetry and ability to stack into layered structures via van der Waals interactions.[1−5] For instance, formations of carbon and inorganic fullerene-like (IF, such as BN, MoS_2, WS_2, etc.) nanotubes have been investigated extensively in recent years.[1−5] Various folding fashions of two-dimensional fullerene-like sheets have been observed and described uniquely with the chirality of nanotubes (wrapping vector and angle), although the actual growth and organization processes of these nanomaterials are still not entirely clear.[1−5]

Apart from the above hollow tubule structures, solid nanorods can also be prepared into one-dimensional crystallite morphology. For example, arrays of ZnO nanorods have been grown along the *c*-axis of the crystal (wurtzite structure) while the C_6 symmetry is strictly maintained for their external crystal facets.[14] Similarly, II−VI semiconductors CdS, CdSe, and CdTe (wurtzite and zinc-blend structures) also show a strong growth anisotropy along the *c*-axis of wurtzite phase.[15−19] On the other hand, one-dimensional materials of groups IV and III−V

* To whom correspondence should be addressed. Email: chezhc@nus.edu.sg.

(1) Iijima S. *Nature* **1991**, *354*, 56.
(2) (a) Ebbesen, T. W.; Ajayan, P. M. *Nature* **1992**, *358*, 220. (b) Ajayan, P. M.; Ebbesen; T. W. *Rep. Prog. Phys.* **1997**, *60*, 1025 and references therein.
(3) Thess, A.; Lee, R.; Nikolaev, P.; Dai, H.; Petit, P.; Robert, J.; Xu, C.; Lee, Y. H.; Kim, S. G.; Rinzler, A. G.; Colbert, D. T.; Scuseria, G. E.; Tomanek, D.; Fischer, J. E.; Smalley, R. E. *Science* **1996**, *273*, 483.
(4) (a) Tenne, R.; Homyonfer, M.; Feldman, Y. *Chem. Mater.* **1998**, *10*, 3225 and references therein. (b) Zak, A.; Feldman, Y.; Alperovich, V.; Rosentsveig, R.; Tenne, R. *J. Am. Chem. Soc*. **2000**, *122*, 11108. (c) Feldman, Y.; Frey, G. L.; Homyonfer, M.; Lyakhovitskaya, V.; Margulis, L.; Cohen, H.; Hodes, G.; Hutchison, J. L.; Tenne, R. *J. Am. Chem. Soc*. **1996**, *118*, 5362.
(5) Nath, M.; Rao, C. N. R. *J. Am. Chem. Soc*. **2001**, *123*, 4841.
(6) Lakshmi, B. B.; Patrissi, C. J.; Martin, C. R. *Chem. Mater*. **1997**, *9*, 2544 and references therein.
(7) (a) Zhang, M.; Bando, Y.; Wada, K. *J. Mater. Sci. Lett.* **2001**, *20*, 167. (b) Zhang, M.; Bando, Y.; Wada, K. *J. Mater. Res.* **2001**, *16*, 1408.
(8) Kobayashi, S.; Hanabusa, K.; Hamasaki, N.; Kimura, M.; Shirai, H. *Chem. Mater*. **2000**, *12*, 1523.
(9) Hippe, C.; Wark, M.; Lork, E.; Schulz-Ekloff, G. *Microporous Mesoporous Mater*. **1999**, *31*, 235.
(10) (a) Hoyer, P. *Langmuir* **1996**, *12*, 1411. (b) Hoyer, P. *Adv. Mater*. **1996**, *8*, 857.
(11) Lencka, M. M.; Riman, R. E. *Chem. Mater.* **1993**, *5*, 61.
(12) (a) Imai, H.; Takei, Y.; Shimizu, K.; Matsuda, M.; Hirashima, H. *J. Mater. Chem*. **1999**, *9*, 2971. (b) Shimizu, K.; Imai, H.; Hirashima, H. Tsukuma, K. *Thin Solid Films* **1999**, *351*, 220. (c) Imai, H.; Matsuda, M.; Shimizu, K.; Hirashima, H.; Negishi, N. *J. Mater. Chem*. **2000**, *10*, 2005.
(13) (a) Kasuga, T.; Hiramatsu, M.; Hoson, A.; Sekino, T.; Niihara, K. *Langmuir* **1998**, *14*, 3160. (b) Kasuga, T.; Hiramatsu, M.; Hoson, A.; Sekino, T.; Niihara, K. *Adv. Mater*. **1999**, *11*, 1307.
(14) Huang, M. H.; Mao, S.; Feick, H.; Yan, H.; Wu, Y.; Kind, H.; Webber, E.; Russo, R.; Yang, P. *Science* **2001**, *292*, 1897.
(15) Li, Y.-D.; Liao, H.-W.; Ding, Y.; Qian, Y. T.; Yang, L.; Zhou, G.-E. *Chem. Mater*. **1998**, *10*, 2301.
(16) Chen, C.-C.; Chao, C.-Y.; Lang, Z.-H. *Chem. Mater*. **2000**, *12*, 1516.
(17) Peng, X.; Manna, L.; Yang, W.; Wickham, J.; Scher, E.; Kadavanich, A.; Alivisatos, A. P. *Nature* **2000**, *404*, 59.
(18) Yang, J.; Zeng, J.-H.; Yu, S.-H.; Yang, L.; Zhou, G.-E.; Qian, Y. T. *Chem. Mater*. **2000**, *12*, 3259.
(19) Jun, Y.-W.; Lee, S.-M.; Kang, N.-J. Cheon, J. *J. Am. Chem. Soc.* **2001**, *123*, 5151.
(20) Wu, Y.; Yang, P. *J. Am. Chem. Soc*. **2001**, *123*, 3165.
(21) Tang, C.; Fan, S. *Adv. Mater.* **2000**, *12*, 1346.
(22) Gudiksen, M. S.; Wang, J.; Lieber, C. M. *J. Phys. Chem. B* **2001**, *105*, 4062.
(23) Liao, H.; Wang, Y.; Zhang, S.; Qian, Y. T. *Chem. Mater*. **2001**, *13*, 6.
(24) Jeevanandam, P.; Koltypin, Yu.; Gedanken, A. *Nano Lett*. **2001**, *1*, 263.
(25) Li, Y.; Sui, M.; Ding, Y.; Zhang, G.; Zhuang, J.; Wang, C. *Adv. Mater*. **2000**, *12*, 818.
(26) Yun, S. K.; Pinnavaia, T. J. *Chem. Mater*. **1995**, *7*, 348.

10.1021/ja012595j CCC: $22.00

semiconductors, such as Si, Ge, GaP, and InP, normally have an axial growth tendency along <111> direction of the diamond or zinc-blend type crystals.[20−22] In all these cases, the growth axes are perpendicular to the highest symmetrical crystallographic planes of the crystals.[14−22]

In contrast to the above cases with hollow cavities, MoS_2 and WS_2, which have hexagonal-layered structures (2H symmetry), can be grown into low-symmetrical crystallites such as elongated nanoplatelets.[23] For instance, one-dimensional MoS_2 nanorods have been synthesized with a preferential one-dimensional growth in solvent-thermal reactions, in which organic ligands are supposed to work as templates in the unidirectional growth, although the actual growth direction has not been determined yet.[23] Natural and artificial minerals and clays, furthermore, represent another group of highly symmetrical materials that show peculiar one-dimensional growth anisotropy.[24−26] In metal hydroxides and double-layered hydroxides (hydrotalcite-like compounds), the basic layered unit possesses hexagonal symmetry (C_6-type), where each divalent metal ion (e.g., $M^{II} = Mg^{2+}$, Ca^{2+}, Co^{2+}, Ni^{2+}) is octahedrally bound to six hydroxyl groups.[27−32] The $M^{II}(OH)_6$ octahedrons share their edges to form two dimensionally infinite brucite-like sheets (brucite $Mg(OH)_2$) which then stack upon one another to form a layered solid via various interlayer chemical interactions.[27−32] Nonetheless, if divalent cations in the $M^{II}(OH)_6$ octahedrons are partially substituted by trivalent ones (e.g., $M^{III} = Al^{3+}$, Co^{3+}, Cr^{3+}), the extra charge of trivalent cations will impose positive charges in the brucite-like sheets.[27−29,31,32] To maintain the overall electrical neutrality, intercalation of anions into the interbrucite-like layers (i.e., interlayer space) has to take place, leading to the formation of a hydrotalcite-like structure (e.g., $Mg_{0.75}Al_{0.25}(OH)_2(CO_3)_{0.125}\cdot 0.5H_2O$).[27−29] Under normal precipitation conditions, the stable crystallite morphology for the above solid compounds is always hexagonal thin platelets perpendicular to the *c*-axis of crystals.[33−38] However, under certain experimental conditions, other less thermodynamically stable morphologies can also be prepared. For example, metal hydroxides can be prepared into fibrous wires of α-$Ni(OH)_2$ with a sonochemical process,[24] one-dimensional nanorods of $Mg(OH)_2$ (brucite) with the assistance of ethylenediamine ligands,[25] and one-dimensional crystallite platelets of $Mg_{1-x}Al_x(OH)_2(CO_3)_{x/2}\cdot nH_2O$ (hydrotalcite) with a variable-pH precipitation method.[26]

It is difficult to comprehend why the hexagonally symmetrical brucite-like sheets in the above metal hydroxides and hydrotalcites can be developed into low-symmetry crystallite morphologies. In this article, we will report a systematic investigation on the ligand-mediated synthesis of brucite-like metal hydroxides, aiming at an understanding on the formation mechanism of the one-dimensional materials. As the basic layered structure in these compounds is the stacks of brucite-like sheets, we have selected the beta-phase cobalt hydroxide, β-$Co(OH)_2$ (hexagonal structure) that has an identical structure to brucite, in the present investigation. In particular, individual and lined assemblies of butterfly-like intermediate nanocrystallites have been stabilized with added ethylenediamine ligands. A direct link between the butterfly-like crystallites and the final one-dimensional β-$Co(OH)_2$ is revealed. In fact, our experimental results indicate that the resultant β-$Co(OH)_2$ nanorods/platelets are comprised of arrays of linearly assembled "butterflies".

Experimental Section

Materials Preparation. The butterfly-like intermediate nanocrystals of β-$Co(OH)_2$ were prepared by ligand-mediated precipitation. In a typical experiment, 5 g of $Co(NO_3)_2\cdot 6H_2O$ (0.017 mol) was transferred to a three-necked round-bottom flask and dissolved by adding 10.0 mL deionized water. The solution was purged with N_2 for 20 min before adding 3.5 mL (0.052 mol) ethylenediamine (En); this gave a Co^{2+} to En molar ratio of 1:3. The resulting solution (pH $\approx$ 10.8) was stirred under flowing N_2 atmosphere at room temperature for 1 h, followed by an addition of NaOH (0.680 M, 50.0 mL) that was divided into two equal parts. In the first half of the addition, 25.0 mL NaOH was added very slowly (dropwise for 1.5 h) into the reaction mixture, which caused a slight turbidity in the solution. The second 25.0 mL NaOH was added fast within 5 min, during which a small amount of (β-$Co(OH)_2$ precipitate (80−100 mg; stage I precipitate) was formed. This precipitate was filtered and washed with deionized water. The clear filtrate was immediately transferred to the round-bottom flask and continuously purged with N_2 gas for 20 min. 50.0 mL of acetone was then added to the filtrate within 6 min, resulting in a large amount of light-pink β-$Co(OH)_2$ precipitate (stage II precipitate). A total of 62−70% of original divalent cobalt had been converted into solid β-$Co(OH)_2$ while the remaining filtrate had a pH $\approx$ 10.2. To prevent the crystallite growth, the precipitate was filtered immediately and washed with deionized water and acetone. All precipitate samples were dried at room temperature under vacuum overnight for further characterization.

Materials Characterization. (1) UV−Visible Measurement. UV−visible absorption spectroscopy measurement was carried out on a Shimadzu UV-3101 PC scanning spectrometer using deionized water as reference. One drop of sample solution was transferred into an airtight quartz UV-cell (2 mL in volume) and diluted with deionized water, followed by the spectrum measurement immediately.

(2) TEM Measurement. Investigation with high-resolution analytical transmission electron microscopy (TEM) was carried out in a JEM-2010 with an electron kinetic energy of 200 kV. The specimens for TEM imaging and selected area electron diffraction (SAED) studies were prepared by suspending solid samples in acetone. About 2−3 mg of sample was added into 3−4 mL acetone in a small glass container that was then placed in an ultrasonic water bath and sonicated for 30−40 min. A drop of this well-dispersed suspension was placed on a carbon-coated 200-mesh copper grid, followed by drying the sample under ambient condition before it was placed in the sample holder of the microscope.

(3) XRD Measurement. The crystallographic information of the samples was investigated by powder X-ray diffraction (XRD). The XRD patterns with diffraction intensity versus 2θ were recorded in a Shimadzu X-ray diffractometer (Model 6000) with Cu K_α radiation (λ = 1.5406 Å) from 5° to 70° at a scanning speed of 2° min^{-1}. X-ray tube voltage and current were set at 40 kV and 30 mA, respectively.[32]

(27) Cavani, F.; Trifiro, F.; Vaccari, A. *Catal. Today* **1991**, *11*, 173 and references therein.
(28) Vaccari, A. *Catal. Today* **1998**, *41*, 53 and references therein.
(29) Rives, V.; Ulibarri, M. A. *Coord. Chem. Rev.* **1999**, *181*, 61 and references therein.
(30) (a) Choy, J. H.; Kwak, S. Y.; Park, J. S.; Jeong, Y. J.; Portier, J. *J. Am. Chem. Soc.* **1999**, *121*, 1399. (b) Sato, H.; Yamagishi, A.; Kawamura, K. *J. Phys. Chem. B* **2001**, *105*, 7990.
(31) Markov, L.; Petrov, K.; Lyubchova, A. *Solid State Ionics* **1990**, *39*, 187.
(32) (a) Chellam, U.; Xu, Z. P.; Zeng, H. C. *Chem. Mater.* **2000**, *12*, 650. (b) Xu; Z. P.; Zeng, H. C. *J. Phys. Chem. B* **2000**, *104*, 10206. (c) Xu; Z. P.; Zeng, H. C. *J. Phys. Chem. B* **2001**, *105*, 1743. (d) Xu, R.; Zeng, H. C. *Chem. Mater.* **2001**, *13*, 297.
(33) Salvadori, B.; Dei, L. *Langmuir* **2001**, *17*, 2371.
(34) Maurel, F.; Hytch, M. J.; Knosp, B.; Backhaus-Ricoult, M. *Eur. Phys. J. AP* **2000**, *9*, 205.
(35) Kannan, S.; Swamy, C. S. *J. Mater. Sci. Lett.* **1992**, *11*, 1585.
(36) Cai, H.; Hillier, A. C.; Franklin, K. R.; Nunn, C. C.; Ward, M. D. *Science* **1994**, *266*, 1551.
(37) Hickey, L.; Kloprogge, J. T.; Frost, R. L. *J. Mater. Sci.* **2000**, *35*, 4347.
(38) Penn, R. L.; Stone, A. T.; Veblen, D. R. *J. Phys. Chem. B* **2001**, *105*, 4690.

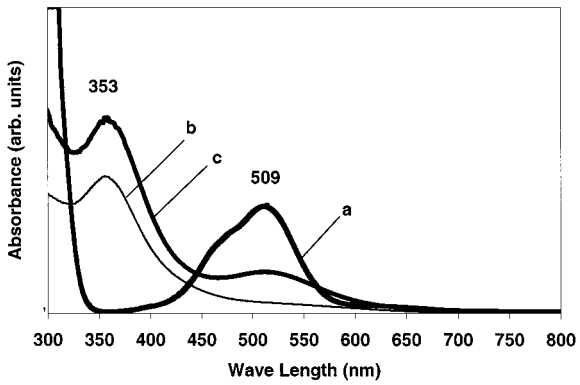

Figure 1. UV−vis spectra for various solution phases: (a) $Co(NO_3)_2$ solution before addition of ethylenediamine or NaOH base, (b) $[Co(En)_3]^{2+}$ solution, and (c) filtrate after stage I precipitation (i.e., prior to the addition of acetone).

(4) TGA/DTG Measurement. About 12−14 mg of each sample was analyzed by thermogravimetric and differential-thermogravimetric analysis (TGA/DTG, Shimadzu TGA-50). The furnace was heated from room temperature to 900 °C at a rate of 10 °C min^{-1} and then cooled naturally. The whole TGA measurement was made under an air atmosphere at a gas flow rate of 50 mL min^{-1}.[32]

(5) CHN Measurement. The weight percentage of carbon and nitrogen in the prepared samples was provided by CHN analysis in a Perkin-Elmer 2400 CHN elemental analyzer.[32]

(6) FTIR Measurement. Ethylenediamine-chelated β-$Co(OH)_2$ powder (before washed) and pure β-$Co(OH)_2$ powder (after washed) were investigated separately with Fourier transform infrared spectroscopy (FTIR; FTS135, Bio-Rad). The potassium bromide (KBr) pellet technique was employed to hold the samples (1 wt %). Each FTIR spectrum was collected after 100 scans with a resolution of 2 cm^{-1}.[32]

Results and Discussion

Figure 1 shows three UV−visible spectra measured for the solution phases at different reaction stages. In this work, the divalent cobalt was first stabilized in the form of $[Co(En)_3]^{2+}$ (orange purple) before a two-step introduction of hydroxide ions.[39] The peak at 353 nm (curve b) is assigned respectively to the d−d transition of $^4T_{1g}(F) \rightarrow {}^4T_{1g}(P)$ (and $^4A_{2g}$) in this octahedral complex (with a large Δ_o, the energy levels of $^4A_{2g}$ and $^4T_{1g}(P)$ are about the same),[40] which is substantially different from that of $[Co(H_2O)_6]^{2+}$ in the initial solution (pink-purple color, the band at ca. 509 nm for $^4T_{1g}(F) \rightarrow {}^4T_{1g}(P)$ in curve a).[41] After introduction of sodium hydroxide (curve c), a new band at ca. 509 nm emerges with a change of solution color to darker orange purple. Because the 353-nm bands in curves b and c are essentially not changed, which indicates there is no appreciable distortion of the octahedral field, we do not consider a transition from $[Co(En)_3]^{2+}$ to $[Co(En)_{3-n}(OH)_n]^{2-n}$ complexes that have elongated octahedral fields.[40] Under the high pH condition, similarly, the broad absorption band at 509 nm cannot be assigned to $^4A_2\ (F) \rightarrow {}^4T_1\ (F)$ transition of T_d symmetry in the tetrahedral complex $[Co(OH)_4]^{2-}$, as this complex has a deep-blue color and should be normally more intense in the visible region (574−630 nm in another blank test for this complex at higher pH conditions).[42] The UV−visible spectrum (not shown) for the filtrate after the major precipitation is essentially the same as curve c. The assignment of the 509-nm band in curve c to $[Co(H_2O)_6]^{2+}$ is supported because the concentration of ethylenediamine had been lowered after major β-$Co(OH)_2$ precipitation (see our later discussion) and formation of the hydrated cobalt cation is expected.

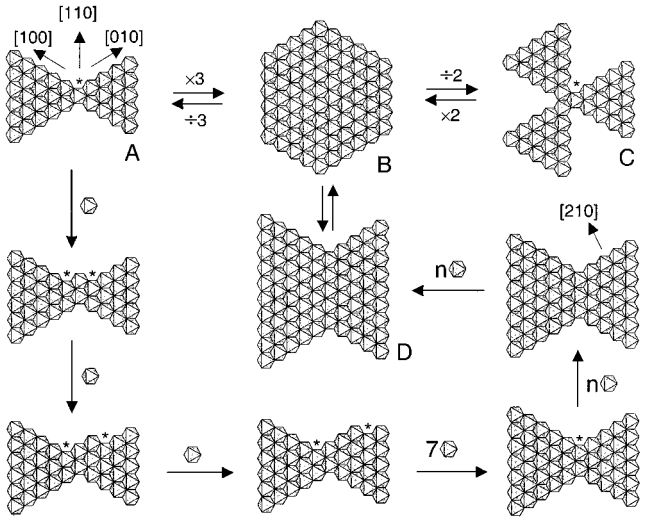

Figure 2. Schematic illustrations of relationships among various structure models. The path from A to D suggests a growth mechanism for the 1D nanorods. The octahedral unit of $Co(OH)_6$ is used to represent growth entity.

Table 1

Structure	Number of equivalent edges	Edge/Area
A	6 × 3 = 18	3
B	6 × 1 = 6	1
C	9 × 2 = 18	3
D	8 × 1 = 8	1.33

On the basis of general geometry, we understand that a hexagon can be divided equally into six smaller triangles with equal edge lengths if the total area is kept constant. In this regard, small triangles can be considered as basic units for constructing other geometrical structures. For example, as shown in Figure 2, joining two triangles in a head-to-head fashion produces three sets of butterfly-like structure A and two sets of fanlike structure C, starting from structure B. On the other hand, structure D can also be constructed from the same six triangles by edge-sharing while keeping the area identical to that of structure B. Table 1 summarizes equivalent edge numbers for the above four different structures taking the total area as a constant. In surface chemistry context, it is understood that a

(39) Norkus, E.; Vaskelis, A.; Griguceviciene, A.; Rozovskis, G.; Reklaitis, J.; Norkus, P. *Transition Met. Chem.* **2001**, *26*, 465.
(40) Cotton, F. A.; Wilkinson, G. *Advanced Inorganic Chemistry*, 6th Ed. (with a chapter on boron by R. Grimes); John Willey & Sons: New York, 1999; Chapter 17, p 820.
(41) Poul, L.; Jouini, N.; Fievet, F. *Chem. Mater.* **2000**, *12*, 3123.
(42) Cotton, F. A.; Wilkinson, G. *Advanced Inorganic Chemistry*; 6th ed. (with a chapter on boron by R. Grimes); John Willey & Sons: New York, 1999; ch. 17, p 816.

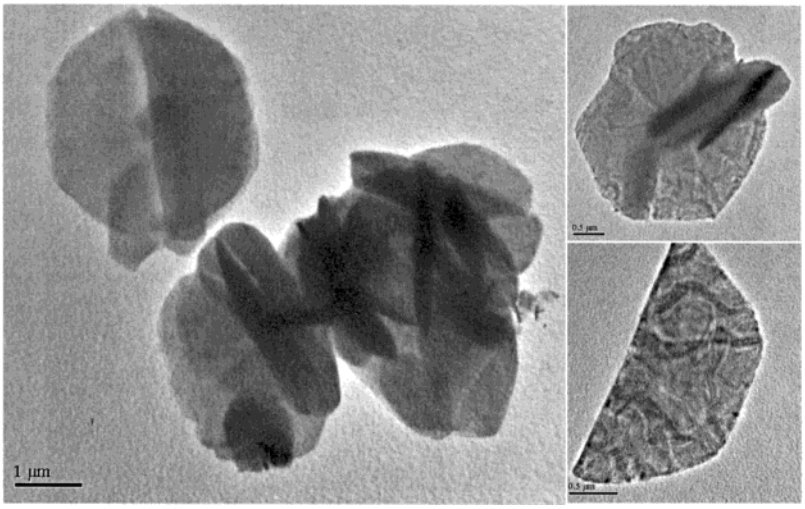

Figure 3. TEM images of hexagonal β-$Co(OH)_2$ platelets and one-dimensional β-$Co(OH)_2$ nanorods formed in stage I precipitation.

high edge/area ratio corresponds to the high system energy for a geometrical system because chemical entities along the edges are undercoordinated, compared to the inner chemical species that are fully bound. According to this, the chemical reactivity of these geometrical structures can be arranged in the following order: C ≈ A > D > B.

Structures with higher system energy are not normally observable, as they are thermodynamically unstable. Presumably, once formed, they will be changed spontaneously to the structures that have lower energy. These transformation processes often occur so fast that they normally give no clues for their intermediate morphologies. It is true that under the normal precipitation conditions, hexagonal crystallites of β-$Co(OH)_2$ (structure B) is the only morphology observed.[33−38] In the current synthesis, a small amount of β-$Co(OH)_2$ was formed when the total NaOH (50 mL) was added but prior to the addition of acetone (i.e., stage I precipitate, see Experimental Section). Our TEM investigation indicates that the β-$Co(OH)_2$ formed at this stage is indeed largely in hexagonal morphology (structure B) because most of the chelating ethylenediamine ligands have not been released yet. Figure 3 shows three TEM images of this type of samples, which indicates that the majority of crystallites are in platelet-like morphology despite some one-dimensional nanocrystallites (dark rods in the images). Because of the presence of ethylenediamine, the observed hexagonal β-$Co(OH)_2$ platelets become very flexible; they can be wrinkled. Interestingly, even half a hexagonal sheet can be preserved (i.e., half of structure B or D). Higher magnified TEM images reveal that the nanorods are tiny "butterflies" stacked exclusively in straight lines. They actually belong to an extended type of structure D, which will be further addressed shortly, and there are no individual butterflies (structure A) at all in these stage I samples.

As mentioned earlier, the major and minor complex species before the addition of acetone were $[Co(En)_3]^{2+}$ and $[Co(H_2O)_6]^{2+}$, respectively. When the acetone was added, some of ethylenediamine ligands were detached from the central cobalt, and a spontaneous precipitation of β-$Co(OH)_2$ was immediately followed, owing to the presence of hydroxide ions and strong chemical miscibility between ethylenediamine and acetone.[43] The nucleation sites for this large-scale precipitation are believed to be the small clusters of β-$Co(OH)_2$ previously formed in the filtrated solution (after adding NaOH in stage I precipitation; see Experimental Section). As shown in the XRD patterns of Figure 4, the precipitates produced in stage II are exclusively in the pure brucite-like phase of β-$Co(OH)_2$; the same XRD pattern is also observed for β-$Co(OH)_2$ formed in stage I (not shown). The interbrucite-sheet distance and lattice-constant *a* (the nearest distance between two Co^{2+} cations within the same brucite-like sheet) are 0.465 and 0.318 nm, respectively, which are identical to the reported data for β-$Co(OH)_2$.[44,45] The elemental analysis indicates that there is no ethylenediamine trapped in the precipitate samples after washing (C% < 0.31% and N% < 0.09%). Thermal decomposition behaviors of β-$Co(OH)_2$ samples are further compared in Figure 5. Because of their small sizes, the β-$Co(OH)_2$ crystallites prepared with the ethylenediamine mediation are easier to be decomposed, which shows a 17 °C difference in decomposition temperature from that of a commercial β-$Co(OH)_2$ sample.[44] Because of higher thermal reactivity, as reported in Figure 5, the decomposed product (cubic phase CoO) from the current work seems to be

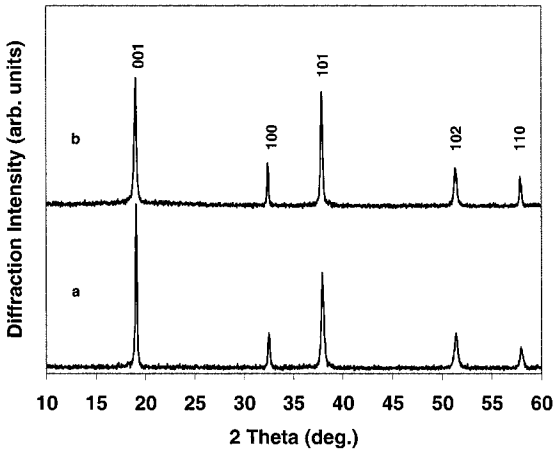

Figure 4. XRD patterns of (a) 100% butterfly-like β-$Co(OH)_2$ formed in stage II precipitation, the same pattern is obtained for samples prepared from stage I precipitation, and (b) commercial β-$Co(OH)_2$ sample (in 100% hexagonal platelets).

(43) Perry, R. H.; Chilton, C. H. *Chemical Engineers' Handbook*; 5th ed.; McGraw-Hill: New York, 1973; pp 3−35.
(44) Xu, Z. P.; Zeng, H. C. *J. Mater. Chem.* **1998**, *8*, 2499.
(45) Xu, Z. P.; Zeng, H. C. *Chem. Mater.* **1999**, *11*, 67.

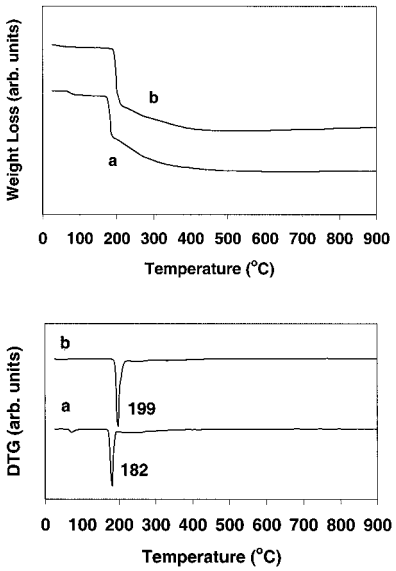

Figure 5. TGA and DTG data for (a) 100% butterfly-like β-$Co(OH)_2$ formed in stage II precipitation and (b) commercial β-$Co(OH)_2$ sample (in 100% hexagonal platelets).

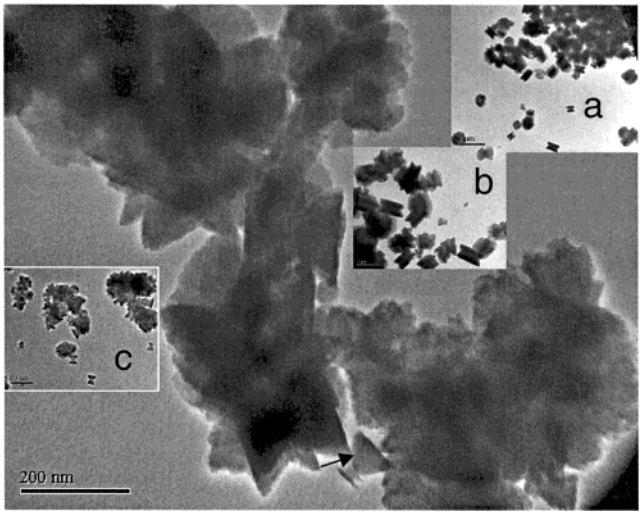

Figure 6. TEM images of aggregates of butterfly-like β-$Co(OH)_2$ formed in stage II precipitation at various magnifications. The arrow indicates a crystallite smaller than 100 nm. Scales in the inserts of a, b, and c are 2 μm, 1 μm, and 0.5 μm, respectively.

able to form a more compact phase, as it is more difficult to be oxidized to spinel Co_3O_4 (i.e., the weight increase over 400−900 °C is less), compared to the commercial sample.[44]

In good agreement with the materials characterization, TEM investigation on the sample morphology indeed indicates the formation of nanosized crystallites in stage II precipitates. Surprisingly, as shown in Figure 6, only one type of butterfly-like crystallite morphology is observed, while the common morphology of hexagonal platelets prepared by conventional methods is totally absent. The observed β-$Co(OH)_2$ butterflies (100% in population) are small-sized, ranging from a few tens nm to about 200 nm. The crystallites often show as aggregates, although free-standing butterflies can be easily prepared with more solvents in sonication, as will be presented shortly. To have a better visual clarity, however, we will only choose the butterflies with a size of 100−200 nm in our later presentation. With the mediation of ethylenediamine, clearly, the originally

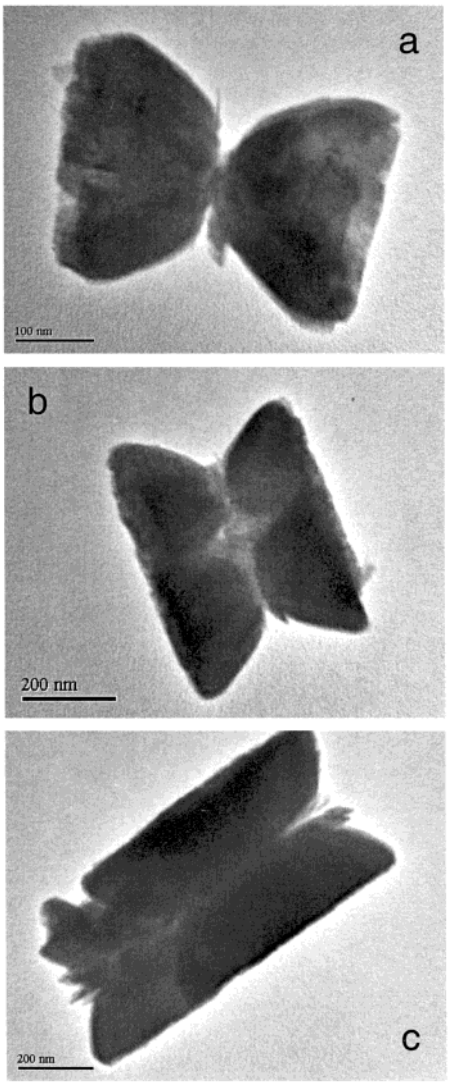

Figure 7. TEM images of free-standing butterfly-like β-$Co(OH)_2$ formed in stage II precipitation: (a) single butterfly, (b) coupled butterflies, and (c) lined butterflies.

unstable forms (e.g., structures A and D) of the crystallites become stable, as evidenced in Figures 3 and 6. With higher concentration of ethylenediamine (such as Co^{2+}:En = 1:3.5), thinner and less-faceted butterflies (not shown) can be prepared with exactly the same procedures. This observation, together with our UV−visible results of Figure 1, suggests that the edges of the butterfly-like crystallites are decorated with the released or excess ethylenediamine ligands. The same two-step synthetic process without adding En (i.e., without En-ligand mediation) can only give normal well-faceted hexagonal β-$Co(OH)_2$ platelets (thicker than those in Figure 3; will be reported in Figure 8c shortly).

In Figure 7, some free-standing butterfly-like crystallites are displayed. They are mostly singled (image 7a), although the butterflies can also be further coupled (image 7b) or aligned into a straight "flying line" (image 7c). In contrast to the lined butterflies, the formation of individual butterflies can be attributed to a sudden release of ethylenediamine by adding acetone, during which localized high concentration may protect these butterflies from further growth. In all cases, nonetheless, "feelers" of the butterflies can be observed clearly at the head

portions, which suggests that there might be some mechanism for the advance along ⟨110⟩ directions. To address this, Figure 2 shows a mechanism for the aligned butterfly formation. Starting from the structure A, one can immediately recognize that there are active sites (marked with an asterisk) located at the central parts which are much less coordinated, compared to other $Co(OH)_6$ octahedrons along the edges. When a new $Co(OH)_6$ octahedron is attached to an active site, two new active sites are generated in both sides of the edges. These active sites are moving along the edges when new $Co(OH)_6$ octahedrons are added, and eventually one whole row of $Co(OH)_6$ octahedrons is added to this growth front. A new active site is regenerated and the next round of addition is followed. The process is carried on repeatedly, and structure A is gradually turned into structure D (Figure 2) that corresponds to the elongated or lined butterflies. This change is thermodynamically favorable because the system energy of a single butterfly is higher than that of lined butterflies (in images 3, 7b, and 7c). The width (along ⟨110⟩) of the aligned butterflies are essentially the same throughout the course of self-assembly while more butterflies are aligned along ⟨110⟩ directions. Alternatively, the feelers of butterflies can be viewed as a smaller-sized structure A that is branching from the central parts of the crystallites (images 7b and 7c). Our model proposed in Figure 2 is thus validated. Further confirmation on crystallographic orientations of the attachment of newly generated $Co(OH)_6$ octahedron has been carried out with selected area electron diffraction (SAED) experiments. In Figure 8a, the selected area of butterfly wing (structure A, Figure 2) and its related diffraction pattern are shown together. The hexagonal pattern can be indexed with diffraction spots belonging to [001] zone. Clearly, the butterfly is single-crystalline lying on the (001) plane, and all observed reflections could be assigned as *hk*0 type. Occasionally, however, additional streaks (at nonintegral positions) to the hexagonal *hk*0 Bragg spots (Figure 8b) are observed, revealing the formation of incommensurate-type superstructures (e.g., CoO in rock-salt-like cubic phase) on the original (001) plane. This observation can be attributed to a topotactic decomposition of the brucite-like layers under electron beam irradiation;[31] the (111) plane of CoO is parallel to the (001) of β-$Co(OH)_2$. As a further example, similar confirmation on crystal orientations for the hexagonal platelets can also be obtained from the SAED result reported in Figure 8c. Two sets of hexagonal diffraction patterns are superimposed with a tilted angle of ca. 12.5°, resulting from the two crystalline platelets (prepared without using En) selected in the measurement.

The wings of the butterflies are well connected although the central parts may be thinner because of the nature of rapid extrusion, as shown in Figure 9a. Continuous planar growth on the (001) plane is also observed, which is reflected in the thickness variation of the butterfly wings, although Oswald-ripening may not be a predominant process in this nonaging synthesis.[46] The dissolution of β-$Co(OH)_2$ during the washing is negligible because of its small K_{sp} (2×10^{-16}).[47] In this agreement, the TEM observation for unwashed samples also shows the same thickness change. However, the ethylenediamine ligands are largely removed during the washing, which is confirmed with the CHN analysis and monitored efficiently with FTIR method for the fingerprint IR absorptions of ethylenediamine at 1053.3 and 3354.6 cm^{-1}.[48] Furthermore, interlayer

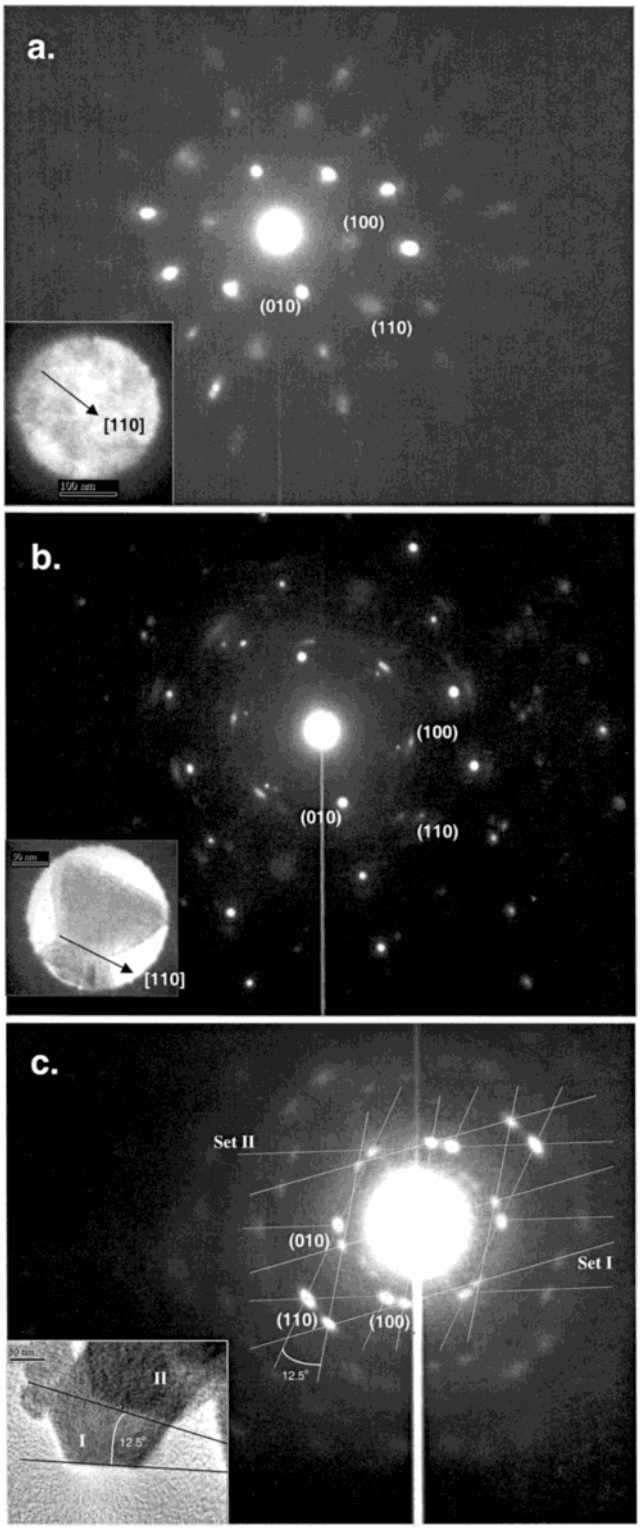

Figure 8. SAED results: (a) hexagonal diffraction pattern from the central part of a butterfly wing, (b) additional spots (streaks) due to incommensurate-type structures, and (c) two hexagonal patterns superimposed with a titled angle of ca. 12.5°. The arrows in all diffraction patterns indicate the butterfly alignment and advancing directions (i.e., ⟨110⟩, Figure 2).

(46) Oswald, W. *Z. Phys. Chem.* **1900**, *34*, 495.
(47) Moeller, T.; Bailar, J. C., Jr.; Kleinberg, J.; Guss, C. O.; Castellion, M. E.; Metz, C. *Chemistry with Inorganic Qualitative Analysis*; Academic Press: New York, 1990; p A23.
(48) Pouchert, C. J. *The Aldrich library of FT-IR spectra*, 1st ed; Aldrich Chemical Co: Milwaukee, WI, 1985; Card No. 24072-9.

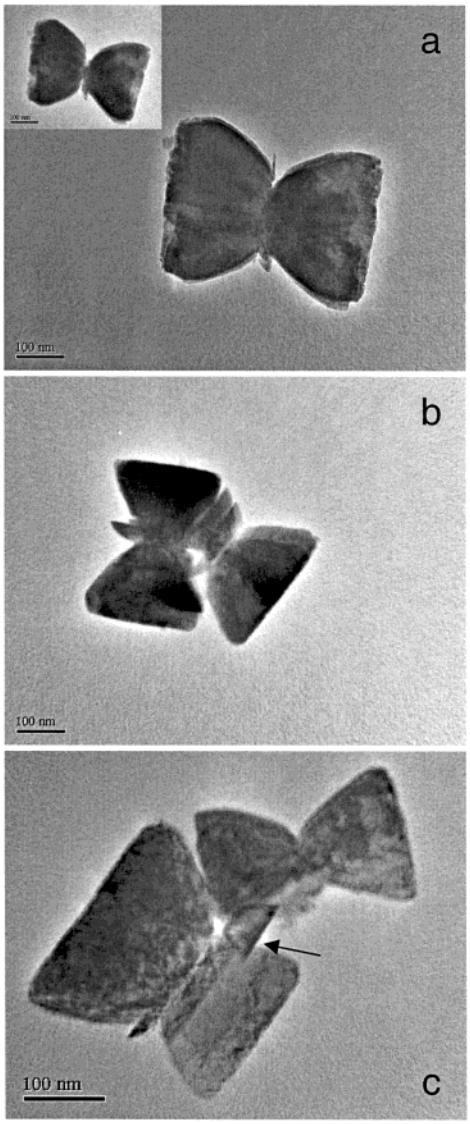

Figure 9. TEM images of rotation and locking in butterfly-like β-Co(OH)$_2$ formed in stage II precipitation: (a) a single butterfly at two different focus levels, (b) 60° rotation, and (c) locking between the two butterflies with a small crystallite (indicated by an arrow).

stacking between β-Co(OH)$_2$ crystallites has been found. In Figure 9b and 9c, two pairs of butterflies are tilted toward each other with an angle of 60°. In both cases, the butterflies should be considered as an integrated piece (belong to the same single-crystalline crystallite) because their C_6 symmetry is strictly maintained. This type of interconnection can be achieved through branching (9b) or locking. As reported in Figure 9c, two butterflies are locked with a small, thin crystallite platelet (marked with an arrow), indicating a cementing mechanism (i.e., combination of primary crystallites[49]) is operative for the butterfly stacking.

Other high-energy crystallites such as structure C (fanlike) are not observed because of the presence of highly undercoordinated sites (Figure 2). These highly active sites can be reproduced rapidly once they are replaced. Therefore, even if it existed in the initial clusters, structure C would quickly change

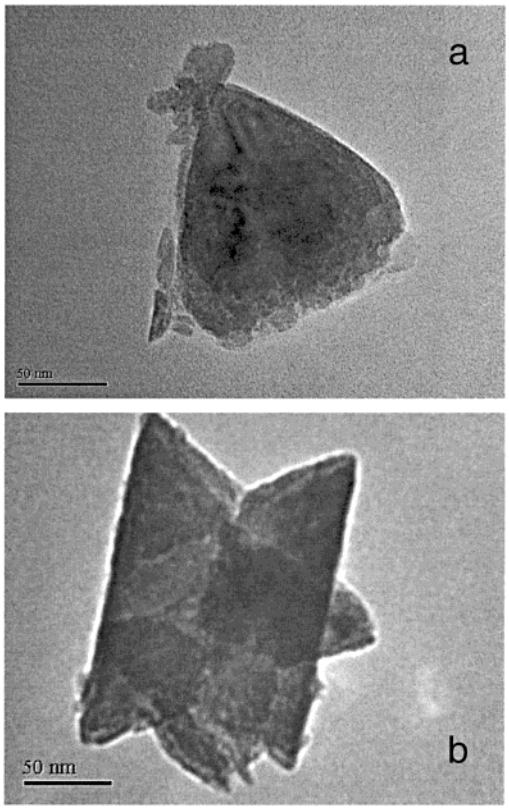

Figure 10. TEM images of triangular bases and extensions in butterfly-like β-Co(OH)$_2$ formed in stage II precipitation: (a) a basic triangle and its extensions and (b) triangular islands formed on a triangle platelet and its related extensions.

to greater triangular shapes, which may further develop into structures A and D (Figure 2). Indeed, the basic unit of triangular crystallites is also found in this study. Displayed in Figure 10 are two triangular crystallites of β-Co(OH)$_2$ of this kind. The single-winged butterfly of image 10a clearly shows a tendency to develop into structure A, although its emerging left wing is much smaller. This tendency is further elucidated in image 10b, in which a triangular crystallite is branched into structure D (lined butterflies). In particular, smaller triangle islands in different thicknesses (darker) can be noticed on the same (001) plane, which reaffirms that the triangle shape is the basic unit in the growth. The growth observed here can be attributed to a new type of branching—in-plane branching that occurs on an existing surface plane; the overall dimension of the triangle is larger than that of the lined butterflies.

Conclusion

In summary, we have demonstrated that, by controlling process parameters, various forms of β-Co(OH)$_2$ crystallites can be prepared at different precipitation stages. In particular, the butterfly-like nanocrystallites in various intermediate modifications can be stabilized in this ethylenediamine-mediated synthesis. By arresting the butterfly-like intermediates, the formed β-Co(OH)$_2$ crystallites can now be understood as different combinations of even smaller building units of triangular platelets. More importantly, the observed linearly aligned butterflies as well as the growth model proposed explain well why a mineral material with C_6 symmetry can be prepared into the form of one-dimensional crystallites (nanorods or nanoribbons). Stacking of butterflies during the precipitation can be

(49) (a) Kolthoff, I. M.; Noponen, G. E. *J. Am. Chem. Soc.* **1938**, *60*, 499. (b) Kolthoff, I. M.; Eggertsen, F. T. *J. Am. Chem. Soc.* **1941**, *63*, 1412. (c) Kolthoff, I. M.; Bowers, R. C. *J. Am. Chem. Soc.* **1954**, *76*, 1510.

explained with a cementing mechanism. In terms of energy isotropy, the observed ⟨110⟩ growth started with a butterfly-like structure is much more advantageous than with a commonly observed hexagonal crystallite. This mode of growth may also be applied to other layered metal hydroxides and clays that have similar hexagonal structures.

Acknowledgment. The authors gratefully acknowledge research funding (R-279-000-064-112 and A/C50384) co-supported by the Ministry of Education and the National Science and Technology Board, Singapore.

JA012595J